Optical and Quantum Electronics (2024) 56:104
https://doi.org/10.1007/s11082-023-05778-6

Properties of MZO/ceramic and MZO/glass thin layers based on the substrate's quality

Dikra Bouras[1,2] · Mamoun Fellah[3,4] · Regis Barille[5] · Mohammed Abdul Samad[6] · Mohammed Rasheed[7] · Maha Awjan Alreshidi[8]

Received: 29 October 2022 / Accepted: 7 November 2023

Abstract
To evaluate the role played by the substrates on the change and the actual difference of the studied samples on their structural, morphological, optical and photocatalytic properties, thin layers of zinc oxide grafted with magnesium were prepared with the same number of layers, doping ratio and experimental conditions with the use of two types of porous ceramic substrates and glassy. The XRD analysis detected the polycrystalline structure with wurtzite-type for all synthesized samples. The grain size was found to vary between 39 and 21 nm for DD3Z and 23 nm to 17 for glass. UV–visible absorbance data indicated that all MZO films absorb visible light at around 410 nm. In addition, a blue shift toward shorter wavelengths side was noted with increasing magnesium content up to 4 wt%, while the band gap showed an increasing trend achieving 3.07 eV for ceramics substrate. SEM analysis showed that the doping greatly affected the morphology of ZnO samples. Based on the results shown by the photocatalytic activities of orange II, the doping with magnesium gave a significant improvement to the samples with a ceramic substrate compared to the samples with a glass substrate. To reveal the mechanism of photolysis Hole/radical scavengers were used. It was found that the addition of Mg–ZnO networks increases the adsorption of hydroxyl ions on the surface and thus acts as a trap site leading to the reduction of hole/electron pair and thus increasing the activity and enhancing photodegradation.

Keywords Mg-doped ZnO/substrats · Photocatalytic · Photodegradation · Nanoparticles

1 Introduction

Semiconductor nanostructures (NSs) are among the most important topics through which broad progress has been achieved in the field of photolysis of water waste and decomposition of water to produce hydrogen (Dingyu et al. 2022; Shabna et al. 2023).

The development of materials in the form of thin layers is of major interest in protection, gas sensors and photovoltaics (Tomar and Garcia 1981). Films deposited in the form of thin layers in particular have physicochemical properties different from those of bulk materials (Francesco et al. 2019). The study of the physical properties of nanostructured materials is of great interest to researchers and industries. Indeed, when we reduce the size

Extended author information available on the last page of the article

of the components of an object down to the nanometric scale, the physical properties of these objects are modified and even improved (Praveenkumara et al. 2023).

Among different materials for semiconductor oxides in thin layers, Zinc oxide, which is the subject of our study is a very potential candidate (You 2015). Zinc oxide (ZnO) is considered to be a transparent type II–VI semiconductor compound, with natural n-type conductivity, characterized by a hexagonal Wurtzite-type structure. Notable properties of ZnO are its forward width of 3.37 eV at room temperature which corresponds to a near ultraviolet (UV) transition and its high exciton binding energy (60 meV) (Balcha and Yadab 2016). ZnO thin films are used in the production of several components and devices, such as gas detectors, solar cells, UV photodetectors, transparent electrodes, piezoelectric transducers and waveguides (Zelalem et al. 2012; Hamidi et al. 2021). The quality of the thin films must be adapted to the desired application, which is a fundamental requirement. This quality can be obtained, either by the conditions of deposition or the production technique (Fellah et al. 2023a).

However, ZnO has a short diffusion length for photogenerated electron–hole pairs during photocatalytic activities which increases the recombination rate of photogenerated electron–hole pairs and leads to decreased photocatalytic activities (Xu et al. 2019; Bouras et al. 2017). This problem can be solved by introducing some metals such as silver, lead, and transition metals such as manganese and cobalt into the ZnO lattice, which reduces the recombination rate of ZnO and at the same time enhances the photocatalytic activity and thus an increase in efficiency can be achieved (Sikder et al. 2021; Fellah et al. 2023b).

There are also other factors that play an important role in enhancing photocatalysis such as phase purity, surface area, crystal size, and preparation method (Asep et al. 2020). Among these elements, magnesium (Mg) is a promising candidate due to its ionic radius similar to that of Zn which allows a high probability of incorporation of Mg^{2+} into the ZnO crystal lattice and can thus increase the absorption wavelength range which will lead to improved degradation efficiency of organic dyes (Chayma et al. 2015; Mohd et al. 2015).

Different techniques such as PVD (physical vapor deposition) and CVD (chemical vapor deposition) (Makhlouf 2011; Luque et al. 2013) can be used to deposit and produce thin layers which are extremely sensitive to the processing conditions. Spray pyrolysis method is one of the most commonly used chemical techniques (Jayesh et al. 2014). This method has the advantage of good control of the doping rate, obtaining large surface layers, speed and simplicity of implementation and low cost (Laura et al. 2012; Muchuweni et al. 2016). The physical methods which consist of producing the film by extracting material from a target among them are the dip-coating (Islam and Azam 2020), spin-coating (Zerouali et al. 2023) and hydrothermal (Jun et al. 2016) methods. The advantage of the physical process is that it is not limited to be used to deposit metal films, compounds, but also alloys (Sabina et al. 2017), ceramics (Bouras et al. 2018), semiconductors (Marwa et al. 2021) and even polymers (Lisanne et al. 2022). This technology is widely applied in industry, aerospace, electronics, optics and mechanics (Abed et al. 2020).

Dip-coating method has been used to prepare magnesium-doped ZnO (Hashim et al. 2017).This method simply consists of immersing the substrate in a solution containing the sol and removing it under very controlled and stable conditions to obtain a film of uniform thickness, and to investigate the photocatalytic performance for the degradation of organic dyes (Pradeev raj et al. 2018).

In this study, we precipitated Mg-doped ZnO using the dip-coating method at low temperature after which heat treatment was carried out at 500 °C and we systematically investigated the effect of Mg-doping on the photocatalytic performance of orange II decomposition under solar irradiation. Furthermore, a kinetic study was performed to understand

the photocatalytic reaction presented in this paper. We concluded that the quality of the substrate plays an important role in increasing effectiveness and improving properties.

2 Experimental details

2.1 Samples fabrication

2.1.1 Porous substrate fabrication

The ceramics used in this work as primary materials are based on local DD3 clay. This material is kaolin obtained from the region of Guelma (Djebel Debagh), has a gray color and is provided by a ceramic company based in Guelma, Algeria. The first one is pure DD3 clay. Its three-mile structure exists naturally in the form of thin sheets and it is a group of quadrilateral layers with eight-faceted layers (Dikra et al. 2020). SiO_2 (> 4 0%) and Al_2O_3 (> 30%) with additional ions, are the most important compounds of the DD3 material (Zerouali et al. 2023). The second material is DD3 clay with 38% of ZrO_2.

After sieving, cylindrical samples (13 mm matrix) were prepared from clay DD3 + 38% ZrO_2. The samples are treated at 1300 °C for 2 h to have thermal transformations which gives us ceramics composed only of mullite–zircon. The presence of zirconium oxide (ZrO_2) leads to the formation of zircon ($ZrSiO_4$) with a high rate of open porosity (33%) after consumption of silica in the vitreous phase (Bouras et al. 2018; Dikra et al. 2020). The ceramics obtained are used as substrates for the thin layers.

2.1.2 Selection of doped element

The main quantity that characterizes zinc oxide is its wide forbidden energy band which limits the creation of thermally activated intrinsic carriers.

Zinc oxide is a material of choice for application in optoelectronic devices such as solar cells and liquid crystal display mirrors (Marwa et al. 2021; Oleksandr et al. 2019). However, ZnO presents application limits in the case of optical devices because its gap is not wide enough (Sizov et al. 2023). This justifies the doping of ZnO with the element Mg to obtain the ternary alloy $Zn_{1-x}Mg_xO$. This new material which exhibits a wider bandgap than ZnO has received great attention due to its potential applications in ultraviolet optoelectronic devices (Nouri 2014). These new thin films, $Zn_{1-x}Mg_xO$ have emerged as one of the important compounds of semiconductors due to the high binding energy and the bandgap which varies between 3.4 eV and ~ 7 eV (Xue et al. 2010).

This difference depends on the Mg addition content. These interesting characteristics allow them to be particularly attractive for applications in devices that operate in the blue-green domain. Many other advantages make $Zn_{1-x}Mg_xO$ an excellent candidate for the future generation of UV light emitting diodes, transparent ohmic contact for solar cells, sensors as well as devices operating at high temperatures and in delicate environments.

2.1.3 Thin layers of Mg-doped ZnO deposition

In a 50 ml cleaned beaker dried in an oven at 50 °C, two witness solutions based on Zinc acetate were prepared. These solutions were used for the dip-coating method. A pure ZnO is formed when the zinc acetate ($Zn(COOCH_3)_2 \cdot 2H_2O$) (Rouchdi et al. 2017) is dissolved

in absolute ethanol. The solution gave us a molar concentration solution of 0.4 mol/l. 4 wt% of Magnesium acetate ($Mg(CH_3CO)_2{\cdot}4H_2O$), was added to one of the two solutions previously prepared. The obtained solutions were mixed using a magnetic stirrer for 2 min at a rotating speed of 500 rpm, with the catalyst ethanolamine (C_2H_7NO) in the ratio of 1:0.

The beaker was left for 2 h at a temperature of 60 °C. The objective of this operation was to obtain a stable and homogeneous solution. During the agitation, the beaker was well covered to prevent any kind of contamination and evaporation of ethanol.

After this preparation of solution, it is deposited on ceramic and glass substrates and we let the sample dry at 200 °C for 5 min. Finally a heat treatment at a temperature of 500 °C for 2 h was performed in order to obtain a crystalline surface. The various steps of this method are shown in the following diagram (Fig. 1a, b).

2.1.4 Sample characterization

The crystal structure and morphology properties of the synthesized pure and Mg-doped ZnO NPs samples were investigated using X-ray powder diffraction (XRD) (Bruker

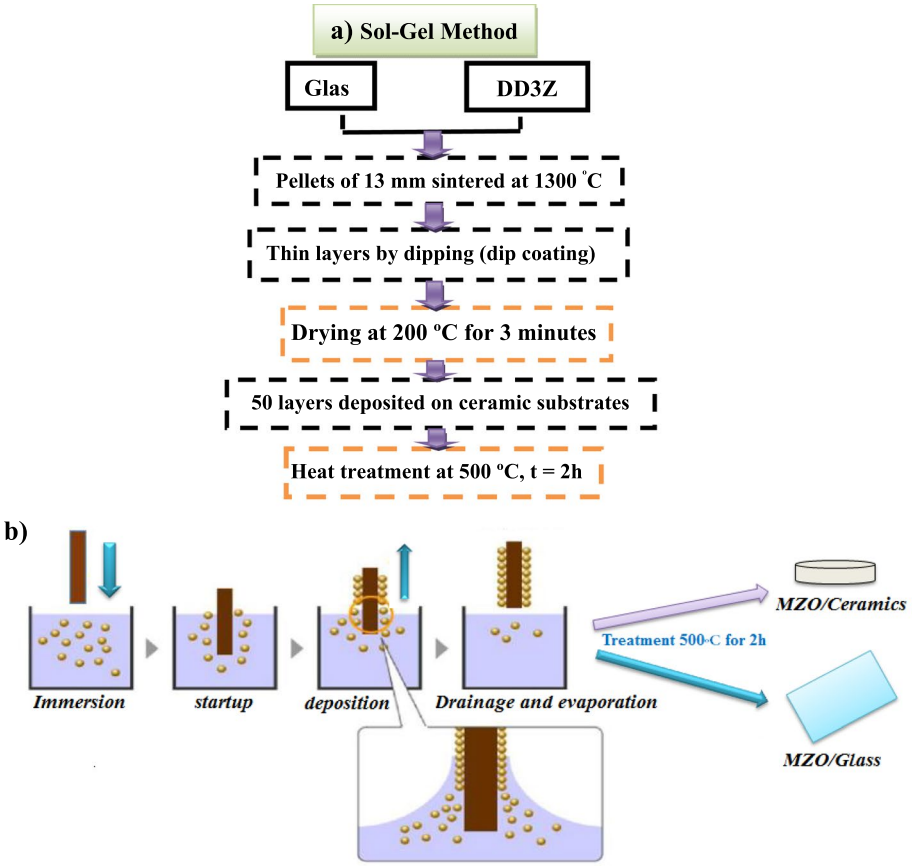

Fig. 1 **a** The main routes followed for the preparation of thin layers with Sol–gel method. **b** Different stages of the dip-coating mechanism

AXS-D8) equipped with (Cu kα)) and field emission scanning electron microscope (FE-SEM) (LEO 1550 Gemini), respectively. The elemental distribution and chemical composition were characterized by energy depressive X-ray (EDX) and atomic force microscope (A100 model of APE Research), respectively. The optical properties were analyzed by UV–vis spectrophotometer (V-630, JASCO) and confocal photoluminescence(Gatan Mono CP4 system combined with Gemini LEO 1550 FE-SEM), respectively.

2.1.5 Structural characterizations

The structural analysis of the ceramic substrates obtained from clay DD3 + 38% ZrO_2 and glass without and with thin layers of ZnO doped with 4 wt% of Mg is carried out by XRD. The results obtained are shown in Fig. 2. From this figure, one can notice that the most intense peaks are obviously those of the ceramic phases (mullite (JCPDS 15-0776), zircon (JCPDS 06-0266), zirconia (JCPDS 37-1484) and cristobalite (JCPDS 39-1425)). In addition to the main phases, there are new peaks appearing at 31.802°, 34.473° and 36.373°, after deposition of the layers. These latter correspond to the planes (100), (002) and (101), respectively of the wurtzite hexagonal phase of the ZnO (JCPDS 03-0891). Concerning the ZnO-doped samples with 4 wt% by weight of Mg, there is a small shift of the spectra with a peak at 43.60° (200) following the MgO phase.

This shift suggests the incorporation of Mg into ZnO crystal lattice in accordance with Vegard's law. Since the ionic radius of Mg^{2+}($r_{Mg}{}^{+2}$ = 0.65 Å) is smaller than that of the Zn^{2+}($r_{Zn}{}^{+2}$ = 0.74 Å), there could be a variation in the lattice constant due to the replacement of Zn^{2+} by Mg^{2+}in the crystal lattice (Yonghong et al. 2016).

Concerning the comparison between the results obtained by the different substrates, difference is at the grain size only (Table 1). Note that the calculation of the grain size may be determined by the Debye–Scherrer relationship (Rouchdi et al. 2017; Yonghong et al. 2016):

$$D = \frac{0.9\lambda}{\beta \cos\theta} \tag{1}$$

where λ is the wavelength of the anticathode (λ_{Cu} = 1.541Å), β is FWHM (half-value width), θ is the diffraction angle and D is the diameter of particle size.

2.1.6 AFM analyses

The AFM technique also makes it possible to visualize the surface of the prepared samples and to analyze statistically the numerical data. That is, it is possible, among other things, to obtain the mean value of the surface roughness (RMS) of these layers. This RMS value is in fact the geometric mean of the heights of all the points of the surface scanned by the microscope. The samples analyzed by AFM are based on DD3Z pellets and glass without and with thin films deposited by dip-coating technique.

The AFM topography of the two substrates is shown in Fig. 3. This figure shows that the distribution of the micropores in the pellets of DD3 + 38 wt% ZrO_2 is non-uniform before doping. The values of their RMS roughness are 100 nm for DD3Z (Table 2). Also the presence of zirconia leads to an open porosity increase in a suitable manner it increases to 22 nm.

Figure 3b, c, e, f shows the AFM topography of the substrates with thin layers of undoped and Mg doped ZnO. It can be noticed from this figure that the surface structure of

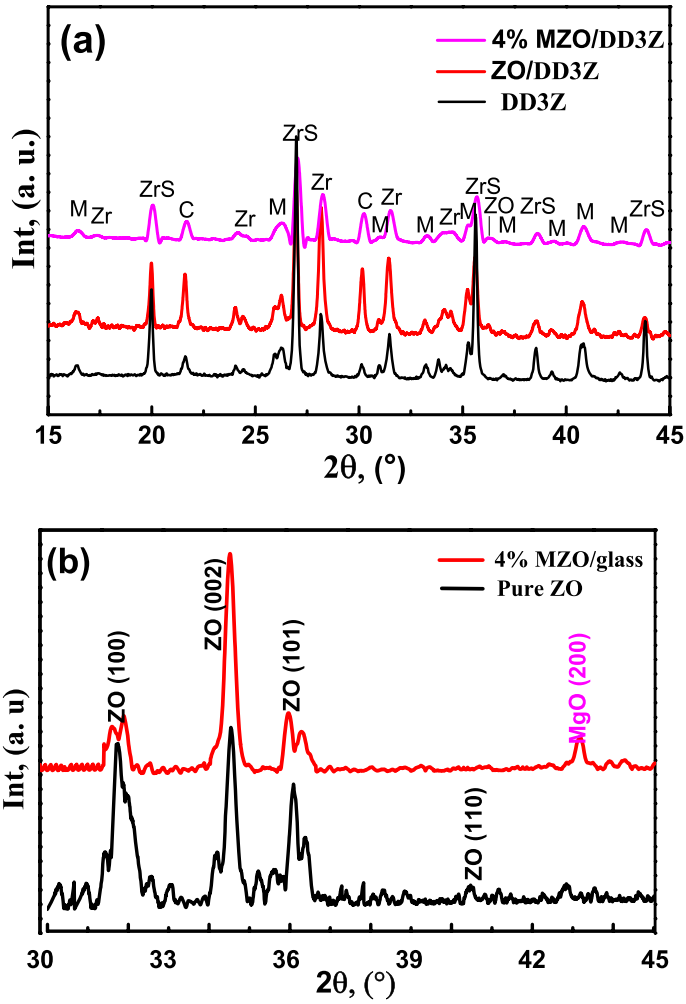

Fig. 2 XRD patterns of thin films of ZnO and Mg doped ZnO deposited on the ceramic and glass substrates: ZrS: Zircon ($ZrSiO_4$), Zr: Zirconia (ZrO_2), C: Cristobalite (SiO_2), M: mullite ($3Al_2O_3{\cdot}2SiO_2$), ZO: ZnO

Table 1 Results of structural analyzes of the DD3Z type before and after deposition MZO thin layers

Phases	(hkl)	2θ (°)	β (°)	D (nm)
Mullite	(210)	26.31	0.352	39
Mullite (MZO)	(210)	26.30	0.653	12
$ZrSiO_4$	(200)	27.01	0.188	43
$ZrSiO_4$ (MZO)	(200)	27.04	0.329	21
ZrO_2	(− 111)	28.19	0.209	37
ZrO_2 (MZO)	(− 111)	28.26	0.351	23
ZnO	(101)	36.23	0.349	23
ZnO/6% Mg	(101)	36.30	0.436	17

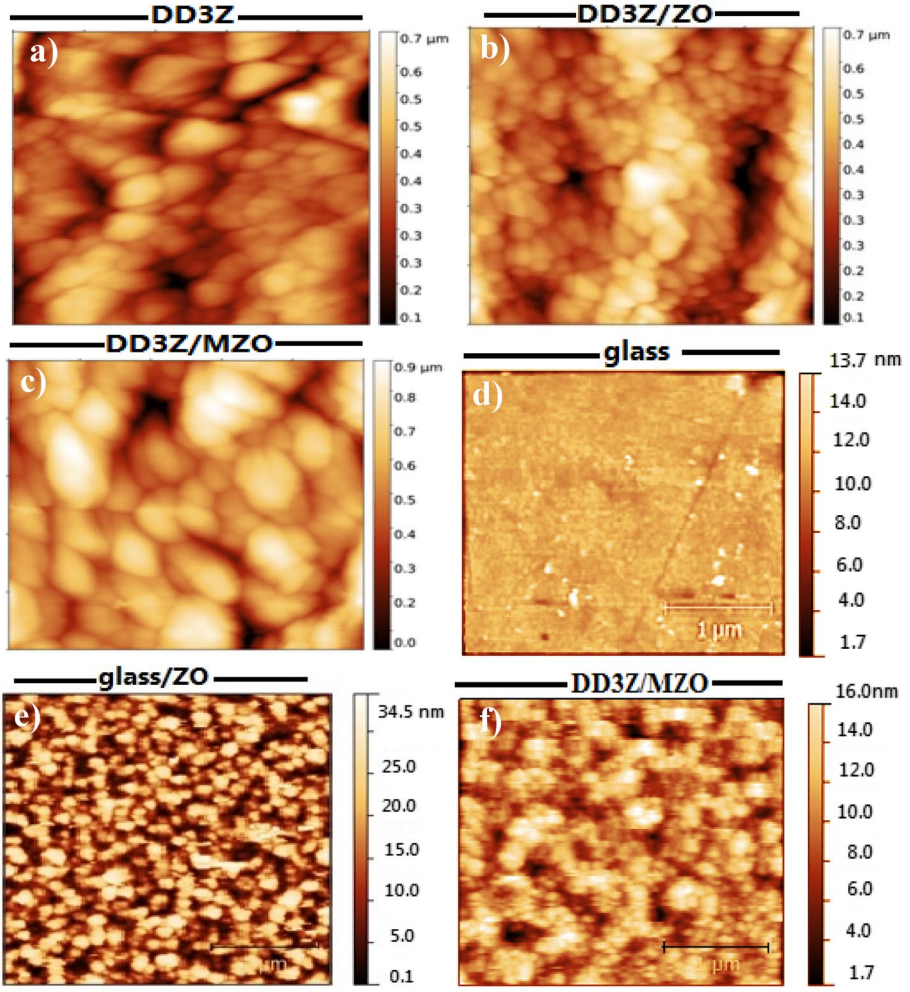

Fig. 3 AFM topography of two different substrates: **a** DD3Z, **b** DD3Z/ZO, **c** DD3Z/MZO, **d** glass, **e** glass/ZO/ and **f** glass/MZO

Table 2 Grain size and the roughness of the samples

Substrates	Ceramic			Glasss		
Samples	DD3Z	ZO/DD3Z	MZO/DD3Z	Glass	ZO/glass	MZO/glass
Grain size (nm)	43	47	25	–	23	16
Roughness (nm)	84	60	108	–	7.50	12.28

the prepared films consists of grains extending upwards. These grains are managed by the growth directions of the ZnO (002)/(100) planes, which are confirmed by the results of the XRD (Fig. 2).

ving the efficiency of these samples for photocatalysis.

This type of growth may lead to obtain an inhomogeneous alignment of the grains of the thin layers. The grain size and roughness (RMS) of the samples are calculated from the AFM topography using Gwiddion software (2.34), the results obtained are shown in Table 2.

The mean value of the surface roughness (RMS), for the substrate DD3Z is 84 nm, while it increases to 108 nm for the same substrates coated with thin layers of ZnO doped with 4 wt% magnesium. The RMS of the substrates of glass without and with the same previous layers increases to 12.28 nm. The large difference in the mean values of the surface roughness between the two types of substrates is due to the presence of the open porosity with different rates.

2.1.7 SEM analysis

Surface morphology study was performed by SEM for MZO/DD3 and MZO/Glass samples. All the thin films showed dense deposition and the surfaces were covered with almost homogeneous and uniform grain size clearly showing crack-free surface formation.

Figure 4a shows that the sample grains before sedimentation are not the same size. But with the presence of steroids; there is a clear change in the shape of the grains after adding

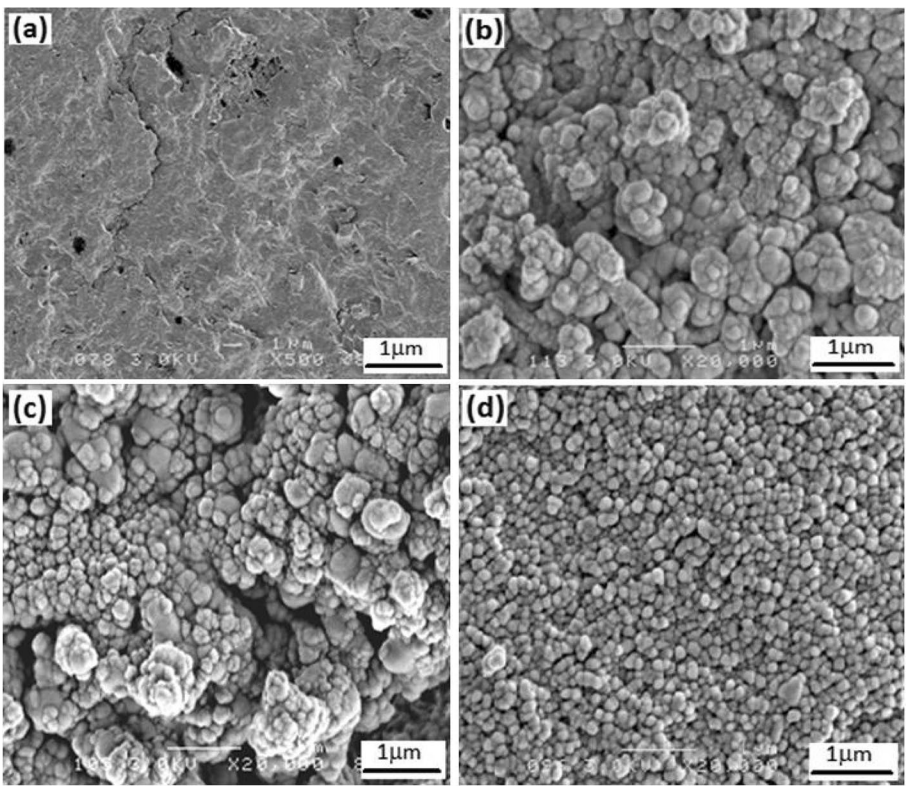

Fig. 4 SEM micrograph of the pellets: **a** DD3Z and **b** ZO/DD3Z, **c** MZO/DD3Z and **d** MZO/glass

Mg, giving them a cauliflower-like appearance. The sample with glass substrate has spherical nanoparticles (Fig. 4c). It is also noted from the SEM images that this change strongly depends on the doping ratio.

Moreover, the presence of larger pores in greater numbers and a significant rate of activation confirm that magnesium gives a more porous surface. An increase in the number and average size of pores was also observed. The value of pore sizes changed from 22 nm (DD3) to 53 nm (with 4 wt% MZO). The addition of magnesium to zinc oxide significantly increased the percentage of pores within the granules and caused a greater number of impurities to be captured in the dye.

2.1.8 EDX analysis

The elemental composition was examined by EDX and Fig. 5a, b confirmed the display of all ceramic peaks as Al, Si, Zr and O. Figure 5b shows the EDX spectrum of the sample doped with 4 wt% Mg which showed a slight presence of Mg at ~ 0.3%. While the basic

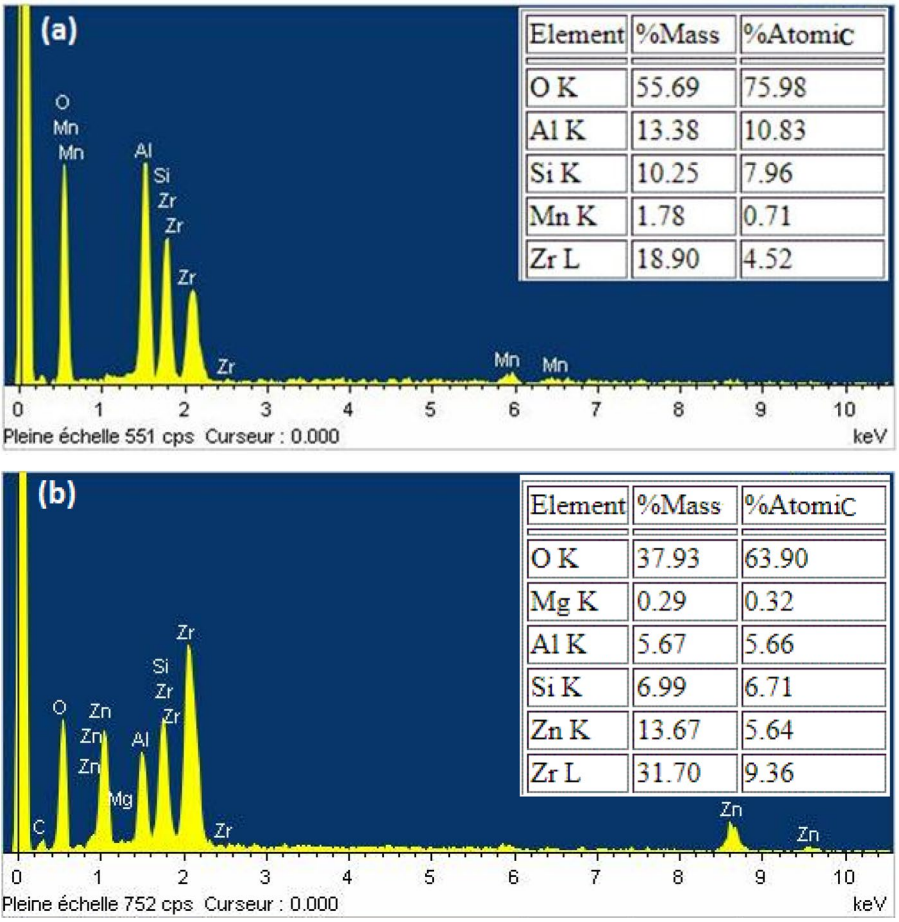

Fig. 5 EDX spectrum of the ceramic pellets: **a** DD3Z and **b** MZO/DD3Z

elemental composition of the ceramic substrates remains such as zirconium, silicium, and aluminum. The magnesium content in the sample doped with 4 wt% magnesium was calculated from the zinc/magnesium ratio and was found to be (2.1 ± 0.4)%, which is less than the expected magnesium percentage in the sample. This could be due to the sedimentation method used or inaccuracy of EDX.

2.1.9 Transmission spectrum and optical energy gap

Transmittance measurements were studied within the wavelength range (200–900 nm) for samples prepared before and after doping with magnesium. The absorbance relationship was plotted as a function of wavelength shown in Fig. 6a, b, and the results showed that the transmittance increases after depositing thin layers on the glass substrate, reaching about ~ 90% (Fig. 6a). While it decreases with deposition in the case of the DD3Z substrate, reaching about ~ 40% (Fig. 6b). This decrease in permeability is attributed to the

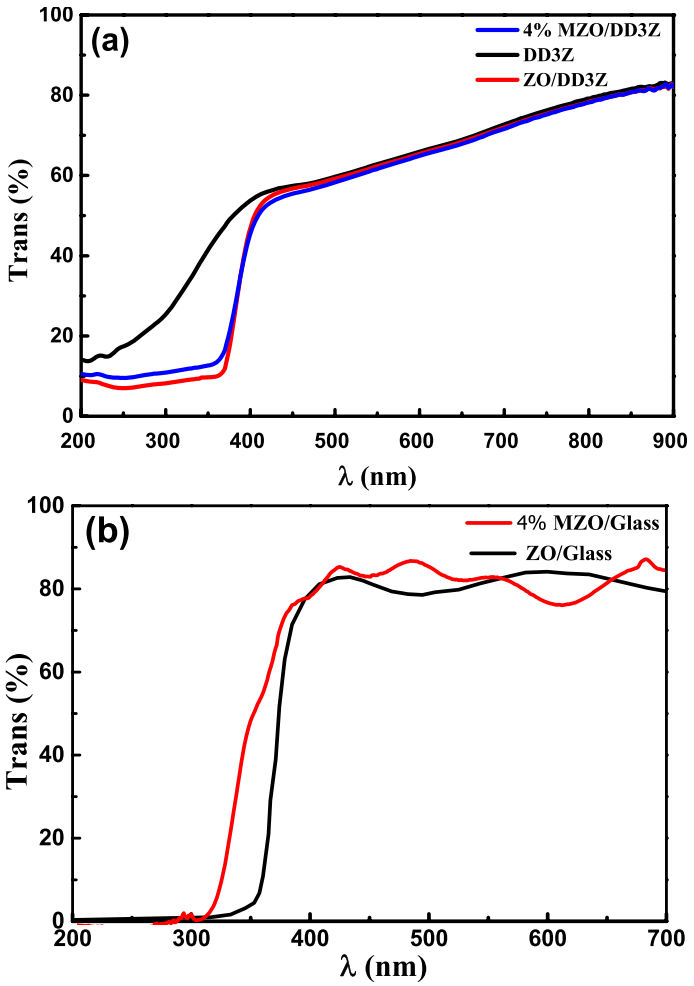

Fig. 6 Transmittance spectra of samples prepared on: **a** ceramic substrates and **b** glass substrates

presence of levels of impurities (magnesium and zinc) within the energy separator, which leads to increased absorption.

To determine the gap energy of the thin layers of samples prepared by the dip-coating method, the following tauc equation is used (Dikra et al. 2023):

$$\alpha h\nu = A \cdot \left(h\nu - E_g\right)^{1/2} \tag{2}$$

with A: Constant, Eg: Optical Gap in eV and hν: The energy of a photon eV.

Figure 7 show the plot of $(\alpha h\nu)^2$ as a function of the energy of a photon $h\nu$ and by the extrapolation method, we have represented the optical gaps E_g.

The plot gives a straight line in the photon energy range, indicating that the samples have a direct electronic transition with a bandgap of 3.72, 3.18, 2.96 and 3.05 eV for DD3Z, 4% MZO/DDZ, glass and 4% MZO/glass respectively (Table 3). The gap energy

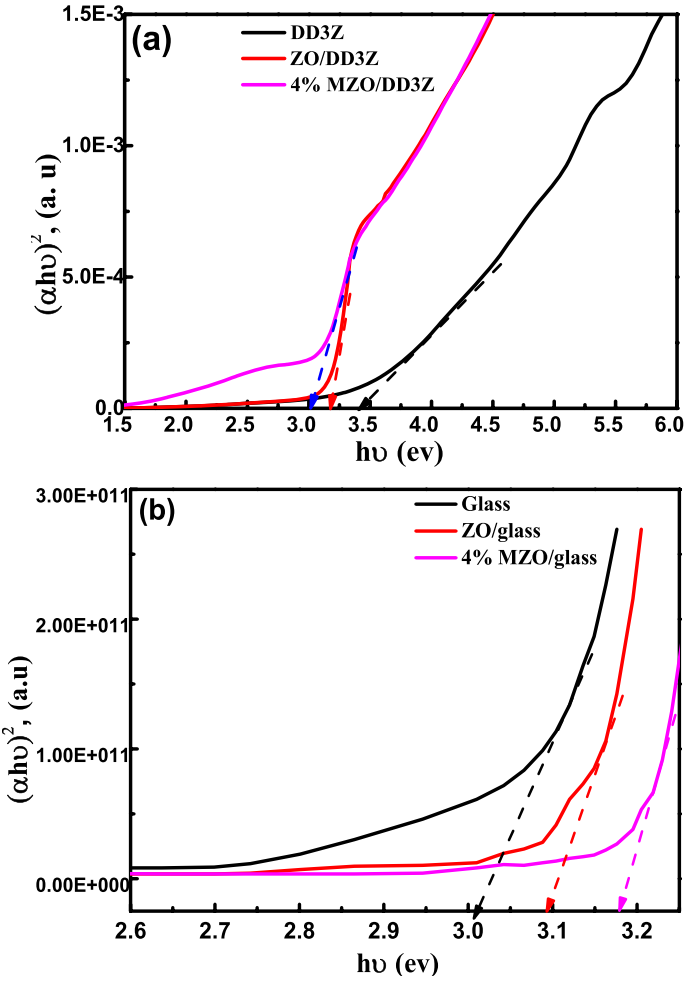

Fig. 7 The values of the energy gaps before and after the deposition of the MZO thin layers: **a** deposited on ceramic, **b** deposited on glass

Table 3 The energy gap of the samples prepared before and after the deposition of the thin layers

	ZO/DD3Z	E_g(eV)
ZO/DD3Z	*DD3Z*	
	Pure DD3Z	3.72
	ZO /DD3Z	3.54
	MZO /DD3Z	3.18
	Glass	
	Glass	2.96
	ZO /glass	3.01
	MZO/glass	3.05

values indicate that it decreases in the case of a ceramic substrate and increases in the case of glass, with Mg doping (Fig. 7). This decrease is explained by the fact that doping leads to a shift of the absorption edge towards lower energies, and this is due to an increase in the energy levels generated above the valence band.

This indicates that the shift of Fermi levels towards the valence gap (VB), which gives the magnesium-doped zinc oxide a *P*-type semiconductor. This leads to the absorption of lower energy photons, and thus to an increase in electronic transitions, and then to a decrease in gap energy values. Therefore, this compound (MZO/DDZ) can be proposed as a photocatalyst under visible light.

An appropriate mathematical analysis of a transmittance spectrum makes it possible to determine the thickness and the void ratio (uncovered surface). Figure 8 shows a quasi-linear growth in the thickness with the deferent thin layers deposited and that the surface becomes completely covered when the number of dips becomes important and also after doping with Mg. The thickness of sample (MZO/Glass) was estimated at 321.29 nm, while we obtained a greater thickness in the case of sample (MZO/DD3Z), which reached 359.36 nm.

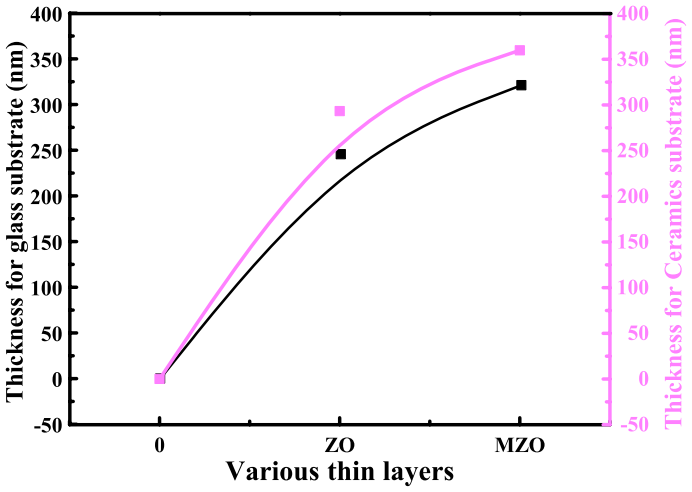

Fig. 8 Thickness of thin layers of samples MZO/DD3Z and MZO/Glass

2.1.10 Confocal spectra

The optical properties of the samples deposited on ceramic substrates were measured with a confocal microscope (Fig. 9).

The confocal device is very sensitive to the quality of the crystal structure and the presence of defects. Band-to-band excitation of ZnO promotes electrons from the valence band to the conduction band, leaving holes in the valence band. Holes migrate from the valence band to deeper levels and recombination occurs between electrons either from the conduction band or shallow donor levels and trapped holes at deep levels (Bouras et al. 2018). Figure 9 shows the confocal spectra of particles before and after thin-layer deposition of Mg:ZnO nanoparticles, with 4 wt% Mg activation. Emission peaks were observed at 441, 465 and 476 nm, and the intensity was found to decrease with thin layers of both zinc oxide and Mg:ZnO.

The decrease in emission intensity with the addition of doping can be attributed to the increase in non-radiative relaxation which is due to the surface-bound states presented by the magnesium ions and the deterioration of the quality of the ZnO crystals and the increase in lattice defects. When the ZnO and MZO layer are deposited, the emission band is broadened and it can be speculated that the ceramic bandwidth is enlarged due to the replacement by Zn^{2+} and Mg^{2+} (Rouchdi et al. 2017).

2.1.11 Measurement of photocatalytic activity

The photocatalytic activity of all the materials was demonstrated by measuring its absorbance of the target material. After the preparation of the aqueous solution of Orange II (12.5 mg/l; pH = 9.6), ZnO thin films doped and deposited on ceramic substrate, we put the samples in direct contact with 25 ml of an Orange II dye solution in under the sunlight. After each 1 h, we took 2.2 ml of the solution in a quartz tube. The absorbance of the solution was analyzed by measuring UV–Vis spectra of in the wavelength range of 250–650 nm. The distilled water was used as a reference.

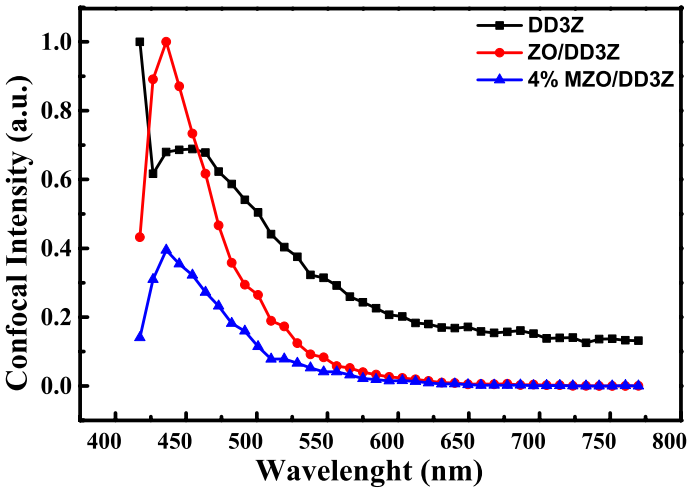

Fig. 9 **a** Confocal spectra of the pellets with ceramics substrates

After each photometric measurement, the photocatalyst was put back to the reaction cell. The absorption rate of degradation was calculated using the following equation (Dikra et al. 2023):

$$\text{Degradation ratio} = \frac{C_0 - C}{C_0} \times 100\% \tag{3}$$

where C_0 and C are the initial concentration before and after illumination respectively.

Photocatalytic experiments were performed under simulated sunlight to investigate the photo-degradation of OII dye for samples with different substrates being pure and Mg-doped. Figure 10 shows the UV–Vis absorption spectra of OII during the photo-degradation reaction time of the samples which are dominated by the main peak of OII centered at 484 nm. As can be seen from Fig. 9, the relative intensity of this peak

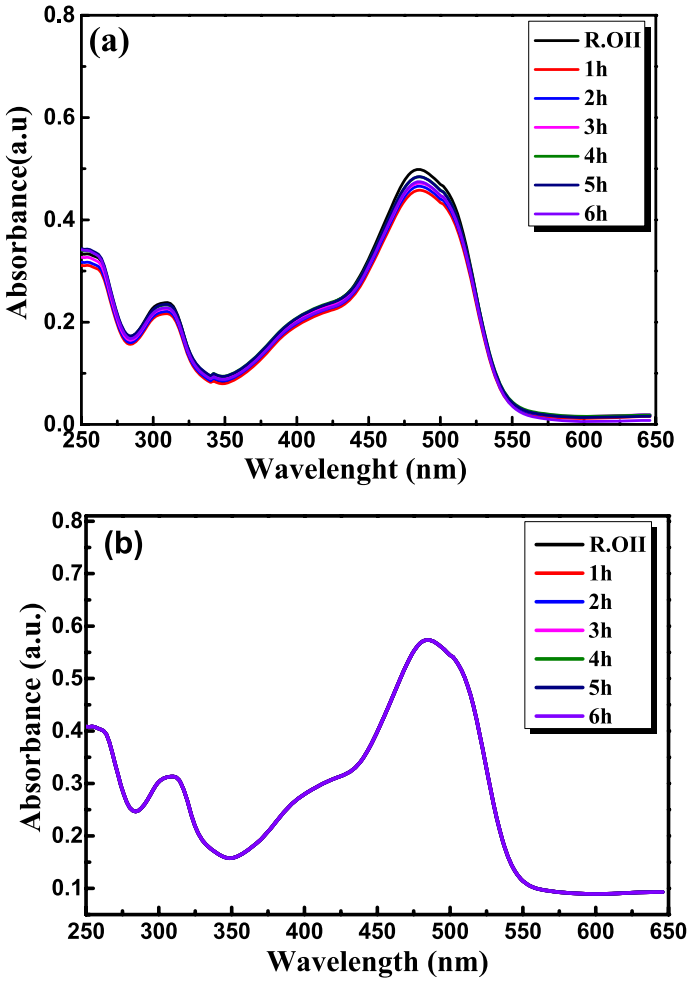

Fig. 10 Degradation rate of Orange II versus UV exposure time for a MZO thin film deposited on a ceramic and glass substrates: **a** DD3Z, **b** glass, **c** MZO/ceramic and **d** MZO/glass

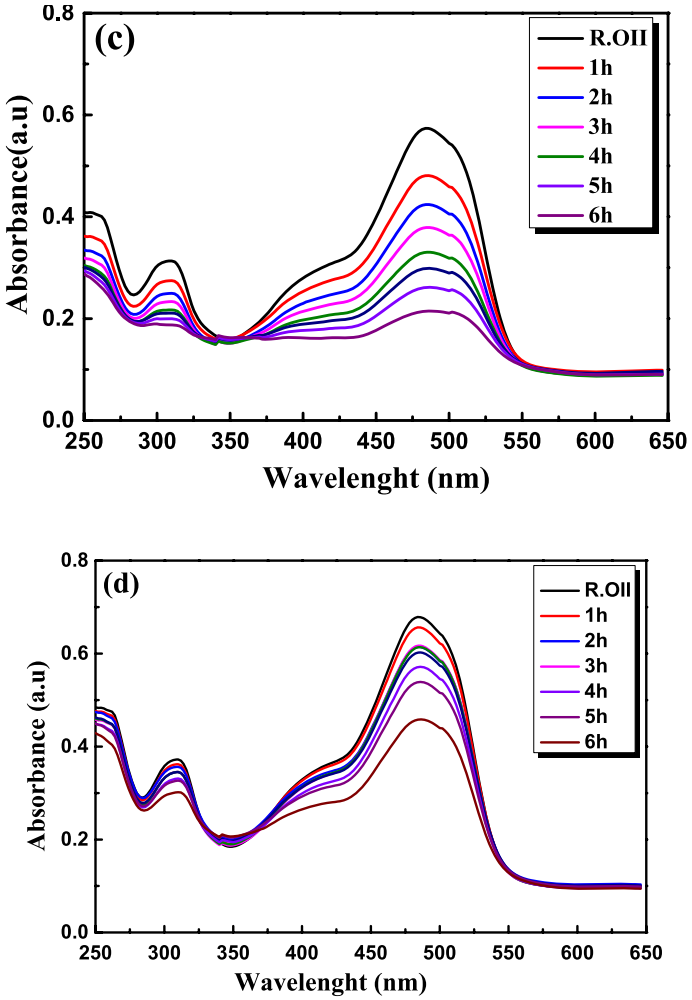

Fig. 10 (continued)

decreases with increasing solar light irradiation time, indicating a degradation of orange II.

The MZO system catalysts with a 4% doping concentration represented greater decomposition efficiency for the ceramic substrate compared to glass, as the decomposition percentage reached 75% and 28.3% (Fig. 11) in a time of 6 h, respectively. The catalyst was faster, which demonstrates the role of the substrate in accelerating the catalysis process and Working to increase the efficiency in decomposing this dye.

Compared to what he found Hira Naseer et al. (2023). It was explored that the photocatalytic activity of all Mg–ZnO/Ag (1%) samples showed maximum degradation of 93% for methylene blue and 87% for rhodamine B. Moreover, the stability of Mg–ZnO/Ag examined after six cycles of regeneration was 83% for MB and 74% for RhB. Therefore, the present work presented a new doped nanocomposite that can be effective in water pollution reduction and various environmental applications (Hira et al. 2023).

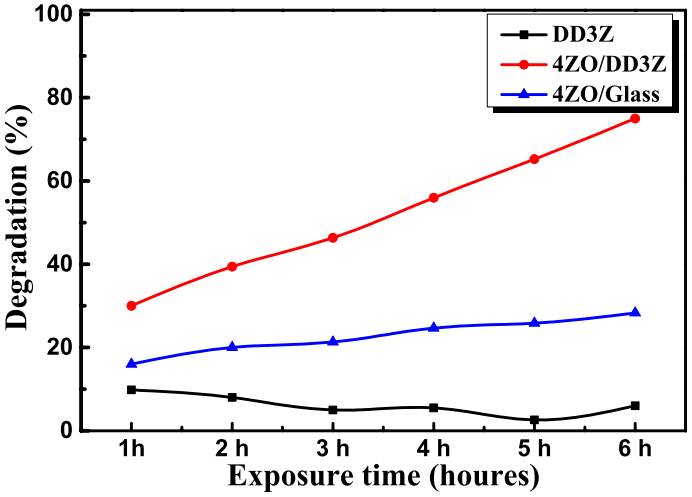

Fig. 11 Comparison of the photocatalytic activity as a function of the exposure time for the two prepared samples: **a** deposited on ceramic, **b** deposited on glass

While Abinash Das et al. (2023) studied the effect of Mg dopant concentration in an experimental and combined density functional theory study on the performance of ZnO simultaneous photo-dye removal and photoelectrochemical water splitting. Mg(3%)–ZnO shows superior photocatalytic performance based on sunlight (Abinash et al. 2023).The work of Qi Zhang et Al. indicates that iron ion content is important for the photocatalytic efficiency of FAZ mesocrystals. Experimental results showed that the optimal molar ratio of Fe^{3+} atoms to Zn atoms was 1%, and the photocatalytic activity of 1FAZ mesocrystals increased by 45% compared with Ag–ZnO obtained under visible light. A possible water purification system was fabricated using a continuous photolysis reactor using FAZ mesocrystals to use solar light as energy to operate the water purification system (Qi et al. 2014). Table 4 shows some of what the researchers achieved while using the compound zinc oxide doped with magnesium (Hira et al. 2023; Abinash et al. 2023; Qi et al. 2014; Imene et al. 2021; Rania et al. 2020; Anand et al. 2019; Labhane et al. 2018; Qiu et al. 2008).

2.1.12 Photocatalytic mechanism

The tested samples for photocatalysis are based on MZO/DD3Z and MZO/glass. In the presence of zirconium oxide in the ceramics, hydroxyl roots (radicals) of ·OH are formed from the latter. For this phenomenon, a pair (e^-/h^+) must be created in the semiconductor by absorbing a photon with energy equal to or greater than the energy gap (Dikra et al. 2022).

The energy gap of the oxides ZnO and MgO, estimated at 3.4 and 7.8 eV, respectively, enables them to generate electron/hole pairs (e^-/h^+) while absorbing light energy (Eq. 1) (Chin et al. 2018). Doping ZnO with Mg resulted in a decrease in recombination and an increase in optical activity in the visual field. Photo-excitation of MZO nanoparticles caused electrons to transition from the valence band to the conduction band leaving behind holes, which is called oxidation–reduction reactions.

Table 4 Comparison of magnesium-doped zinc oxide to previous work on photo-degradation of organic dyes

Photocatalyst	Source of light	Synthesis method	Heat treatment	Dye	Degradation	References
Mg–ZnO/Ag	UV	Ultrasonic waves	–	MB and RhB	83% and 74%	Hira et al. (2023)
Mg-doped ZnO	UV	Sol–gel technique	500 °C	MB	90% for 330 min	Imene et al. (2021)
3% Mg–ZnO	Solar light	Sol–gel technique	550 °C	MB	90% for 80min	Abinash et al. (2023)
Mg-doped ZnO NPs	Solar light	Co-Precipitation method	–	MB	98% for 120 min	Rania et al. (2020)
ZnO–MgO	Solar light	Co-Precipitation Method	600 °C	RhB	83% for 90 min	Anand et al. (2019)
Mg/ZnO–GO	Solar light	Co-precipitation Method	550 °C	Pnitrophenol	97% for 60 min	Labhane et al. (2018)
$Zn_{1-x}Mg_xO$ nanostructures	UV	Wet chemical Method	350 °C	MB	90% for 300 min	Qiu et al. (2008)
4%Mg doped ZnO	Solar light	Sol–gel technique	500 °C	OII	75% for 360 min	Current work

From electrons in the conduction band interacting with molecular oxygen to produce superoxide radical ions $\cdot O_2^-$ and hydroperoxyl radicals $\cdot HO_2^-$ (Eq. 2) (Mohamed 2021), while holes are trapped in the valence band in space from hydroxyl ions to create OH· radicals (Eq. 3). Creation of more OH· and $\cdot HO_2^-$ resulted in high oxidation, factors that contributed to the attack and dissociation of the organic dye molecules (Eq. 4, 5) (Mohamed 2021). The separation and migration mechanism of the photo-generated electron/hole pairs of the MZO sample through a schematic illustration (Fig. 12).

In ZnO and MgO electrons can reduce O_2 to $\cdot O^-{}_2$due to their negative CB edge potential of (−0.41 and −3.20 eV) with respect to the standard redox potential $E^{\Theta}(O_2/\cdot O_2^-)$ (−0.33 eV vs. NHE) (Bouras et al. 2021). Thus, the process begins when holes react with water to produce hydroxide, and electrons react with oxygen to cause a transparent color of the polluted solution. $\cdot O^-{}_2$ may then react with H_2O to form $\cdot HO_2$ and$\cdot H_2O_2$ (Chin et al. 2018). Moreover, due to the valence band edge location of both ZnO and MgO oxides (+2.92 eV for ZnO and +4.6 eV for MgO), there is a possibility of dye oxidation to CO_2 and H_2O with ZnO and MgO through the aforementioned holes (Chin et al. 2018; Mohamed 2021). The position values of two semiconductors at the zero charge point are calculated using the following relations (Bouras et al. 2021; Hezil and Fellah 2019; Fellah et al. 2015):

$$E_{BV} = X - E_e + 0.5E_g \tag{4}$$

$$E_{BC} = E_{BV} - E_g \tag{5}$$

where E_{VB} is the potential of the valence band edge, and E_{CB} is the potential of the conduction band edge, X is the electro-negativity value (X_{ZnO} = 5.79 eV, X_{MgO} = 5.215 eV), E_e is the energy of free electrons at the level of hydrogen (~4.5 eV) and Eg is the band width of the semiconductor (Dikra et al. 2023). The role of magnesium doping is very effective compared to the case of ZnO, it increases the rate of ·OH in a very noticeable way, The formation of holes depends on the chemical nature of MZO which can explain the high

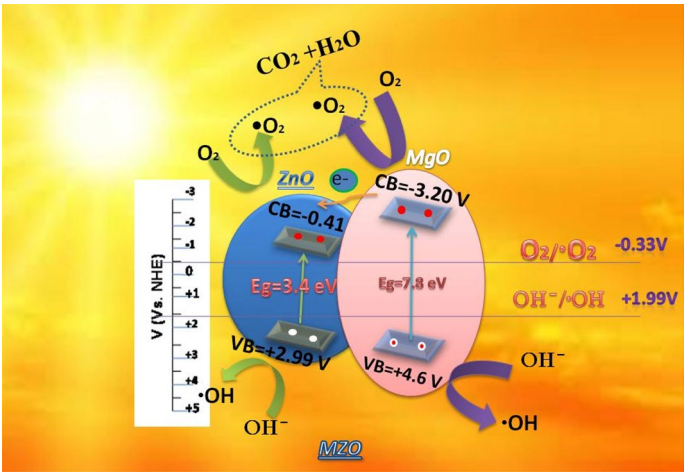

Fig. 12 The photocatalytic mechanism of MZO thin layers under visible light

degradation rate of the dye Orange II in samples upon magnesium inoculation. Here are the chemical equations:

$$\mathrm{ZnO} + \mathrm{MgO} + \mathrm{hu} \rightarrow \mathrm{ZnO}\,(\mathrm{e}^-) + \mathrm{ZnO}\left(\mathrm{h}^+\right) + \mathrm{MgO}\,(\mathrm{e}^-) + \mathrm{MgO}\left(\mathrm{h}^+\right) \quad (6)$$

$$\mathrm{ZnO}\,(\mathrm{e}^-) + \mathrm{MgO}\,(\mathrm{e}^-) + \mathrm{O_2} + \mathrm{H_2O} \rightarrow \cdot\mathrm{O_2^-} + \cdot\mathrm{HO_2^-} \quad (7)$$

$$\mathrm{ZnO}\left(\mathrm{h}^+\right) + \mathrm{MgO}\left(\mathrm{h}^+\right) + \mathrm{OH}^- + \mathrm{H_2O} \rightarrow \mathrm{OH}\cdot \quad (8)$$

$$\mathrm{OH}\cdot + \mathrm{Dey} \rightarrow \text{mineralization dye} \quad (9)$$

$$o\mathrm{O} + \cdot o\mathrm{HO_2^-} \cdot + \textit{mineralizationdye} \cdot \mathrm{CO_2} \cdot + \mathrm{H_2O} \quad (10)$$

3 Conclusions

Thin ZnO layers saturated with 4 wt% Mg were deposited on ceramic and glass substrates using the sol–gel method to prepare purification elements in our daily lives at low cost. The effect of these dopants on the structural activity, shape, and photocatalytic thin layer was studied. The morphology of the outer layers is studied by atomic force microscopy; it was found that increasing the concentration of magnesium as well as increasing the level of open porosity in the substrate leads to a higher surface roughness. From the SEM results, it was observed that there were pores in the case of Mg grafting in both types of substrates with cauliflower-like protrusion on the ceramic surface. The photocatalytic activity on Orange II is carried out under sunlight by pellets, where a 12.5 mg/l aqueous solution was used. The degradation rate of Orange II was 77.76% for 6 h. These good results were obtained from samples prepared from DD3 clay with ZrO_2 and zinc oxide doped with 4 wt% Mg. This important effect could be related to the high rate of open porosity in these substrates. The presence of open porosity makes the specific surface larger and is then filled with zinc oxide and copper oxide and contributes to the deposition of a larger amount of impurities in the polluted solution. The maximum degree of purification obtained is 75% with an improvement rate of 6 h, while it reached 28.33% for the glass substrate during the same period of time.

Acknowledgements This work has been supported by the Laboratory of MOLTECH-Anjou, Angers University, France.

Author contributions DB Original draft, Supervision, Visualization, Resources. MF Data curation, Writing- Original draft preparation. Conceptualization, Methodology and Software Reviewing and Editing. RB Reviewing and Editing. MAS Writing- Reviewing. MR Reviewing and Editing. MAA Data curation

Declarations

Conflict of interests The authors declare no competing interests.

References

Abed, C., Fernández, S., Elhouichet, H.: Studies of optical properties of ZnO: MgO thin films fabricated by sputtering from home-made stable oversize targets. Optik **216(4–6)**, 164934 (2020)

Abinash, D., Dongyu, L., Riu, W., Andrey, S.V., Oleg, V.P., Ranjith, G.N.: Enhancement of photocatalytic and photoelectrochemical performance of ZnO by Mg doping: experimental and density functional theory insights. J. Phys. Chem. Lett. **14**(18), 4134–4141 (2023)

Anand, K.V., Aravind Kumar, J., Keerthana, K., Deb, P., Tamilselvan, S., Theerthagiri, J., Rajeswari, V., Sekaran, S.M.S., Govindaraju, K.: Photocatalytic degradation of rhodamine B Dye using biogenic hybrid ZnO–MgO nanocomposites under visible light. Chem. Select. **4**, 5178–5184 (2019)

Asep, B.D.N., Rena, Z., Rosi, O.: Correlation between crystallite size and photocatalytic performance of micrometer-sized monoclinic WO_3 particles. Arab. J. Chem. **13**(1), 1283–1296 (2020)

Balcha, O.P., Yadab, T.D.: Photocatalytic degradation of methylene blue dye by zinc oxide nanoparticles obtained from precipitation and sol-gel methods. ESPR **23**, 25485–25493 (2016)

Bouras, D., Mecif, A., Mahdjoub, A., Harabi, M., Zaabat, M., Barille, R.: Photocatalytic degradation of orange II by active layers of cu-doped ZnO deposited on porous ceramic substrates. J. Ovonic Res. **13**, 271–281 (2017)

Bouras, D., Mecif, A., Barille, R., Harabi, A., Rasheed, M., Mahdjoub, A.: Cu:ZnO deposited on porous ceramic substrates by a simple thermal method for photocatalytic application. Ceram. Int. **44**(17), 21546–21555 (2018)

Bouras, D., Mecif, A., Harabi, A., Barillé, R., Mahdjoub, A., h Zaabat M: Economic and ultrafast photocatalytic degradation of orange II using ceramic powders. Catalysts **11**(733), 1–22 (2021)

Chayma, A., Chaker, B., Habib, E., Bernard, G., Mokhtar, F.: Mg doping induced high structural quality of sol–gel ZnO nanocrystals: application in photocatalysis. Appl. Surf. Sci. **349**, 855–863 (2015)

Chin, B.O., Law, Y.N., Abdul, W.M.: A review of ZnO nanoparticles as solar photocatalysts: synthesis, mechanisms and applications. Renew. Sust. Energ. Rev. **81**, 536–551 (2018)

Dikra, B., Mecif, A., Barille, R., Harabi, A., Zaabat, M.: Porosity properties of porous ceramic substrates added with zinc and magnesium material. Ceram. Int. **46**, 20838–20846 (2020)

Dikra, B., Rasheed, M., Barille, R., Mustafa, N.: Efficiency of adding DD3+(Li/Mg) composite to plants and their fibers during the process of filtering solutions of toxic organic dyes. Opt. Mat. **131**, 112725 (2022)

Dikra, B., Fellah, M., Abla, M., Régis, B., Aleksei, O., Mohammed, R.: High photocatalytic capacity of porous ceramic-based powder doped with MgO. J. Korean Ceram. Soc. **60**, 155–168 (2023)

Dingyu, L., Chengwu, Y., Saravanan, R., Jiaqian, Q., Xinyu, Z.: Nanoflower-like $Ti_3CN@TiO_2$/CdS heterojunction photocatalyst for efficient photocatalytic water splitting. Int. J. Hydrogen Energy **47**(45), 19580–19589 (2022)

El Hamidi, A., El Mahboub, E., Meziane, K., El Hichou, A., Almaggoussi, A.: The effect of electronegativity on optical properties of Mg doped ZnO. Optik **241**, 167070 (2021)

Fellah, M., Abdulsamad, M., Labaïz, M., Assala, O.: Sliding friction and wear performance of the nanobioceramic α-Al_2O_3 prepared by high energy milling. Tribol. Int. **91**, 151–159 (2015)

Fellah, M., Hezil, N., Bouras, D., Obrosov, A., Abdul, S.M., Montagne El Din, S., Weiß, S.: Structural mechanical and tribological performance of a nano structured biomaterial Co–Cr–Mo alloy synthesized via mechanical alloying. J. Mater. Res. Technol. **25**, 2152–2165 (2023a)

Fellah, M., Hezil, N., Bouras, D., Khalifa, A.-W., H: Investigating the effect of milling time on structural, mechanical and tribological properties of a nanostructured hiped alpha alumina for biomaterial applications. Arab. J. Chem. **16**(17), 105112 (2023b)

Francesco, B., Shridhar, J., Christos, P., Bowers, J.W., Walls, J.M., Munshi, A.H., Barth, K.L., Sampath, W.S.: Degradation of Mg-doped zinc oxide buffer layers in thin film CdTe solar cells. Thin Solid Films **691**, 137556 (2019)

Hashim, N.H., Subramani, S., Devarajan, M., Ibrahim, A.R.: Properties of undoped ZnO and Mg doped ZnO thin films by sol–gel method for optoelectronic applications. J. Aust. Ceram. Soc. **53**, 421–431 (2017)

Hezil, N., Fellah, M.: Synthesis, structural and mechanical properties of nanobioceramic (α-Al_2O_3). J. Aust. Ceram. Soc. **55**, 1167–1175 (2019)

Hira, N., Nabil, A., Tahir, I., Muhammad, Y., Sumera, A., Muhammad, S.S., Ismail, W., Muhammad, F., Arslan, M.: Investigation of Mg doped ZnO nanoparticles decorated with Ag for efficient photocatalytic degradation. J. Inorg. Organomet. Polym. Mater. **33**, 2790–2802 (2023)

Imene, A., Boubekeur, B., Mouloud, L., Malak, K., Valérie, B., David, H., Miloud, S., Ouhiba, H.: Influence of magnesium doping on microstructure optical and photocatalytic activity of zinc oxide thin films synthesis by sol–gel route. Appl. Phys. A **127**, 1–14 (2021)

Islam, M.R., Azam, M.G.: Enhanced photocatalytic activity of Mg-doped ZnO thin films prepared by sol–gel method. Eng. Surf. **37**(6), 775–783 (2020)
Jayesh, P., Frej, M., Abdellah, A., Devendra, T., Tapas, K.C.: Spin-coating deposition of PbS and CdS thin films for solar cell application. Appl. Phys. A **117**, 1791–1799 (2014)
Jun, Y., Yongqian, W., Junhan, K., Meihua, Y., Hongyun, J.: Synthesis of Mg-doped hierarchical ZnO nanostructures via hydrothermal method and their optical properties. J. Alloys Compd. **657**, 261–267 (2016)
Labhane, P.K., Sonawane, S.H., Sonawane, G.H., Patil, S.P., Huse, V.R.: Influence of Mg doping on ZnO nanoparticles decorated on graphene oxide (GO) crumpled paper like sheet and its high photo catalytic performance under sunlight. J. Phys. Chem. Solids **114**, 71–82 (2018)
Laura, M.M., Alexandru, E., Anca, D.: Influence of spray pyrolysis deposition parameters on the optoelectronic properties of WO_3 thin films. Thin Solid Films **520**(13), 4282–4290 (2012)
Lisanne, D., Matthias, B., Katrin, U., Paola, P., Mauro, G., Anna, M.C.: Shedding light on the initial growth of ZnO during plasma-enhanced atomic layer deposition on vapor-deposited polymer thin films. Appl. Surf. Sci. **604**, 154619 (2022)
Luque, P.A., Quevedo-Lopez, M.A., Olivas, A.: Influence of deposition time on ZnS thin film growth over SiO_2 and glass substrates. Mater. Lett. **106**, 49–51 (2013)
Makhlouf, A.S.H.: 1—Current and advanced coating technologies for industrial applications, nanocoatings and ultra-thin films technologies and applications woodhead. Publishing series in metals and surface engineering, pp. 3–23 (2011)
Marwa, K.A., Mohammed, A.F., Al Salihi, H.A., Abdulmajeed Salbi, H.A.: Effect of ZnO nanoparticles deposition on porous silicon solar cell. Mater. Today Protoc. **42**, 2935–2940 (2021)
Mohamed, F.: Plant-mediated biosynthesis and photocatalysis activities of zinc oxide nanoparticles: a prospect towards dyes mineralization. J. Nanotechnol. **1**, 1–15 (2021)
Mohd, A., Meenhaz, M.A., Arham, S.A., Pushpendra, T., Ashraf, S.S.Z., Naqvi, A.H., Ameer, A.: Band gap engineering and enhanced photoluminescence of Mg doped ZnO nanoparticles synthesized by wet chemical route. J. Lumin. **161**, 275–280 (2015)
Muchuweni, E., Sathiaraj, T.S., Nyakotyo, H.: Effect of gallium doping on the structural, optical and electrical properties of zinc oxide thin films prepared by spray pyrolysis. Ceram. Int. **42**, 10066–10070 (2016)
Nouri, H., Habibi-Yangjeh, A.: Microwave-assisted method for preparation of $Zn_{1-x}Mg_xO$ nanostructures and their activities for photodegradation of methylene blue. Adv. Powder Technol. **25**(3), 1016–1025 (2014)
Oleksandr, D., Oleksii, D., Maksym, K., Andriy, S., Serhii, V., Peter, B., Sergei, P., Anatoliy, O.: Morphological, structural and optical properties of Mg-doped ZnO nanocrystals synthesized using polyol process. Mater. Sci. Semicond. Process. **102**, 104595 (2019)
Pradeevraj, K., Sadaiyandi, K., Kennedy, A., Sagadevan, S., Chowdhury, Z.Z., Johan, M.R.B.: Influence of Mg doping on ZnO nanoparticles for enhanced photocatalytic evaluation and antibacterial analysis. Nanoscale Res. Lett. **13**, 1–13 (2018)
Praveenkumara, J., Sanjay, M.R., Suchart, S.: Advanced characterization techniques for nanostructured materials in biomedical applications. Adv. Ind. Eng. Polym. Res. (2023). https://doi.org/10.1016/j.aiepr.2023.03.002
Qi, Z., Jin-Ku, L., Jian-Dong, W., Hong-Xi, L., Yi, L., Xiao-Hong, Y.: Atmospheric self-induction synthesis and enhanced visible light photocatalytic performance of Fe^{3+} doped Ag–ZnO mesocrystals. Ind. Eng. Chem. **53**(34), 13236–13246 (2014)
Qiu, X., Li, L., Zheng, J., Liu, J., Sun, X., Li, G.: Origin of the enhanced photocatalytic activities of semiconductors: a case study of ZnO doped with Mg^{2+}. J. Phys. Chem. C **112**, 12242–12248 (2008)
Rania, E.A., Hatim, A., Galia, P., Xianjie, L., Magnus, W., Omer, N.: Synthesis of Mg-doped ZnO NPs via a chemical low-temperature method and investigation of the efficient photocatalytic activity for the degradation of dyes under solar light. Solid State Sci. **99**, 106053 (2020)
Rouchdi, M., Salmani, E., Fares, B., Hassanain, N., Mzerd, A.: Synthesis and characteristics of Mg doped ZnO thin films: experimental and ab-initio study. Res. Phys. **7**, 620–627 (2017)
Sabina, A.H., Ghada, H.D., Ammar, N.: Effect of atomic layer deposited Al_2O_3:ZnO alloys on thin-film silicon photovoltaic devices. J. Appl. Phys. **122**(24), 245103 (2017)
Shabna, S., Dhas, S.J., S Biju CS: Potential progress in SnO_2 nanostructures for enhancing photocatalytic degradation of organic pollutants. Catal. Commun. **177**, 106642 (2023)
Sikder, A.A., Md Muktadir, B., Sadiq, S.N., Alamgir, K.: Enhanced photocatalytic activity of Ho^{3+} doped ZnO NPs synthesized by modified sol-gel method: an experimental and theoretical investigation. J. Alloys Compd. **856**, 158217 (2021)

Sizov, F., Tsybrii, Z., Rudenko, E., Svavilnyi, M., Kyrychok, T., Kolomys, O., Vuichyk, M., Svezhentsova, K., Skoryk, M., Strelchuk, V., Maziar, D., Gudymenko, O., Polotskiy, D., Panarin, V., Korotash, I.: ZnO nanorods on conductive substrates. Technol. Featur. Nano-Struct. Nano-Objects **35**, 101013 (2023)

Tomar, M.S., Garcia, F.J.: Spray pyrolysis in solar cells and gas sensors. Prog. Cryst. Growth Charact. Mater. **4**(3), 221–248 (1981)

Xu, T., Xing, W., He, H., Zhang, D., Zhang, N., Xiao, Z., Tao, H.: Self-assembly method assisted synthesis of g-C_3N_4/ZnO heterostructure nanocomposites with enhanced photocatalytic performance. Opt. Mater. **96**, 109266 (2019)

Xue, L., Xaing, L., Peng-Ting, L., Xing-Wang, C., Ying, L., Chuan-Bao, C.: Mg doping reduced full width at half maximum of the near-band-edge emission in Mg doped ZnO films. Chin. Phys. B **19**, 027202 (2010)

Yonghong, H., Haibo, Z., Jifu, D., Ziyu, H., Shengli, Z.: The structural, electrical and optical properties of Mg-doped ZnO with different interstitial Mg concentration. Mater. Chem. Phys. **182**, 15–21 (2016)

You, H.C.: Transistor characteristics of zinc oxide active layers at various zinc acetate dihydrate solution concentrations of zinc oxide thin-film. J. Appl. Res. Technol. **13**(2), 291–296 (2015)

Zelalem, N., Urgessa, O.S., Oluwafemi, J.R.B.: Hydrothermal synthesis of ZnO thin films and its electrical characterization. Mater. Lett. **79**(15), 266–269 (2012)

Zerouali, M., Daira, R., Dikra, B., Boudjema, B., Régis, B.: Photocatalytic degradation of orange II by active layers of Ag-doped CuO deposited by spin-coating method. J. Nano Res. **80**, 1–19 (2023)

Authors and Affiliations

Dikra Bouras[1,2] · Mamoun Fellah[3,4] · Regis Barille[5] · Mohammed Abdul Samad[6] · Mohammed Rasheed[7] · Maha Awjan Alreshidi[8]

✉ Dikra Bouras
bouras.dhikra@yahoo.fr

✉ Mamoun Fellah
mamoune.fellah@univ-khenchela.dz

[1] Faculty of Science and Technology, University of Souk-Ahras, Souk Ahras, Algeria

[2] Laboratory of Active Components and Materials, Larbi Ben M'hidi University, 04000 Oum El Bouaghi, Algeria

[3] Mechanical Engineering Department, ABBES Laghrour University, PO 1252, CP 40004 Khenchela, Algeria

[4] Biomaterial, Synthesis and Tribology Research Team, ABBES Laghrour-University, P.O 1252, 40004 Khenchela, Algeria

[5] MOLTECH-Anjou, Université d'Angers/UMR CNRS 6200, 2 Bd Lavoisier, 49045 Angers, France

[6] Mechanical Engineering Department and IRC-AM, King Fhad University of Petroleum and Minerals, 31261 Dhahran, Saudi Arabia

[7] Applied Sciences Department, University of Technology- Iraq, Baghdad, Iraq

[8] Departement of Chemistry, University of Ha'il, 81441 Ha'il, Saudi Arabia